La mer 33, 77-87, 1995
Société franco-japonaise d'océanographie, Tokyo

A numerical experiment on the path dynamics of the Kuroshio south of Japan Part 2. Bottom topographic effect*

Mingqiu ZHANG** and Yoshihiko SEKINE**

Abstract: On the basis of the results of Part I (Zhang and Sekine, 1995), effects of bottom and coastal topographies on the path dynamics of the Kuroshio south of Japan are investigated by using of a two layer model. The realistic coastal and bottom topographies south of Japan are modeled and twelve experiments with different bottom slope, different volume transport of in- and outflow and different coefficient of horizontal eddy viscosity are performed. In the cases with the realistic bottom topography and relatively large horizontal eddy viscosity ($A_h=10^7$ cm^2sec^{-1}), current path flows along northern boundary and the large meander path is not formed. As for these cases, main vorticety balance is made between the divergence term and coupling term, which indicates the stability of the current path over the continental slope. This tendency is also detected in the cases with decreased bottom slope (half ~ 1/10 of the realistic bottom slope). However, formation of large meander path is carried out in the model with relatively small eddy viscosity ($A_h=5\times10^6 cm^2sec^{-1}$), decreased bottom slope (1/10) and large in- and outflow volume transport of 80 Sv. In this case, large kinetic energy in the lower layer is generated by the occurrence of baroclinic instability and the main vorticity balance is made among advection, divergence and coupling terms, which shows the increase in the inertial effects in comparison with the cases with large eddy viscosity. It is suggested that the large meander path is made by the baroclinic instability under strong inertial condition.

1. Introduction

The Kuroshio south of Japan has two representative current paths between straight path and large meander path. In Part 1 of the present study (ZHANG and SEKINE, 1995), the coastal topographic effect was examined by use of a two layer flat bottom model. As the succeeding study of Part I, we further investigate the bottom topographic effect on the path dynamics of the Kuroshio. There have been various studies on the bottom topographic effect: if effects of friction and density stratification are neglected, a geostrophic flow has a very strong tendency to be vertically coherent flow and runs along f/h contours, where f is Coriolis parameter and h total depth of the ocean (e.g. PEDLOSKY, 1979). Here, because change in f is relatively small in local flow dynamics, the flow actually runs along isopleths of h. If effects of density stratification is considered, the tendency of vertical coherence is weakened.

In the regions of the Kuroshio south of Japan, there exist various bottom topographies such as the continental slope and the Izu Ridge. Most of the previous studies on the path dynamics of the Kuroshio have been focused on the coastal topographies and intensity of volume transport (current velocity) (e.g. WHITE and MCCREARY, 1976; CHAO and MCCREARY, 1982; CHAO, 1984; YOON and YASUDA, 1987; SEKINE, 1988; YAMAGATA and UMATANI, 1989; AKITOMO *et al.*, 1991). However, bottom topographic effects have not been fully discussed in the previous studeies. SEKINE (1990) investigated the bottom topographic effect south of Japan. However, because the straight northern coastal boundary topography is assumed in SEKINE (1990), path dynamics of the Kuroshio was not fully discussed. In this study, we examine the coastal and bottom topographic

* Received December 7, 1994
** Institute of Oceanography, Faculty of Bioresources, Mie University, 1515, Kamihama, Tsu, Mie, 514 Japan

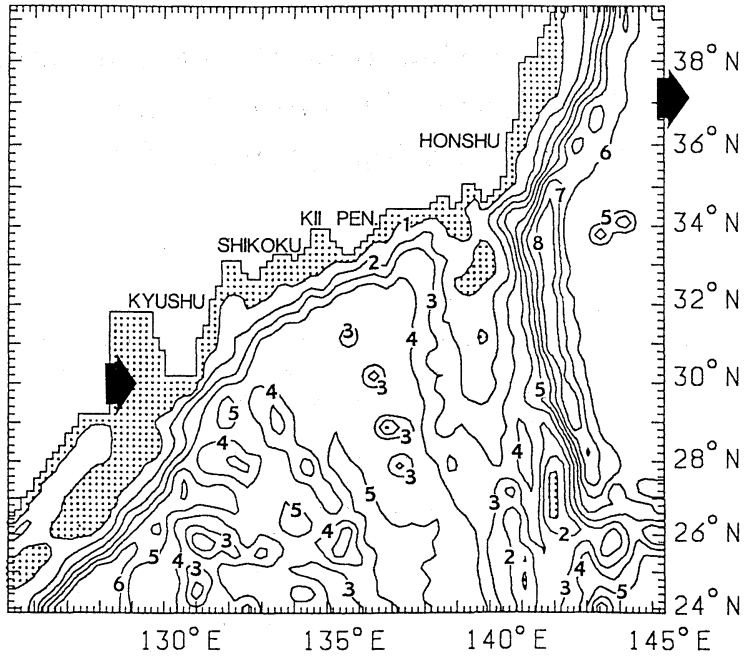

Fig. 1. Model basin. Contour of isobar is shown by every 1000 m. Regions with depth shallower than 1000 m are stippled.

effects on the path dynamics of the Kuroshio by use of a numerical model with realistic coastal and bottom topographies south of Japan.

2. Model

A two layer ocean with bottom and coastal topographies shown in Fig. 1 is employed. Here, coastal boundaries are the same as those in Part I and only the realistic bottom topographies south of Japan are added. The basic equations are the same as those in Part I, except for the vorticity equation. Because of the inclusion of bottom slope, two topographic terms, divergence and coupling terms, are added in the vorticity equation: the divergence term estimates total divergence or convergence of upper and lower layer over the bottom slope, while the coupling term estimates stretching or shrinking between the interface gradient and bottom slope. The vorticity equation is as follows (for all the symbols, see Table 1 of Part 1):

In- and outflow systems, initial and boundary conditions are also the same as those in Part I. In the present study, twelve runs with different bottom topographies, horizontal eddy viscosity, and in- and outflow volume transport are performed (Table 1). Here, mean depth of the model ocean is assumed to be 3800

$$\boxed{\frac{\partial Z}{\partial t}} = \boxed{\begin{aligned} &-\frac{\partial}{\partial x}\left\{\frac{1}{D}\left(\frac{\partial}{\partial x}u_1\nu_1 h_1+\frac{\partial}{\partial y}\nu_1^2 h_1\right)\right\}+\frac{\partial}{\partial y}\left\{\frac{1}{D}\left(\frac{\partial}{\partial x}u_1^2 h_1+\frac{\partial}{\partial y}u_1\nu_1 h_1\right)\right\}\\ &-\frac{\partial}{\partial x}\left\{\frac{1}{D}\left(\frac{\partial}{\partial x}u_2\nu_2 h_2+\frac{\partial}{\partial y}\nu_2^2 h_2\right)\right\}+\frac{\partial}{\partial y}\left\{\frac{1}{D}\left(\frac{\partial}{\partial x}u_2^2 h_2+\frac{\partial}{\partial y}u_2\nu_2 h_2\right)\right\}\end{aligned}} \text{ Advection}$$

Total change

$$\text{Beta term } \boxed{-\frac{\beta\partial\phi}{D\partial x}} \qquad \boxed{+f\left\{\frac{\partial}{\partial x}\left(\frac{1\partial\phi}{D\partial y}\right)-\frac{\partial}{\partial y}\left(\frac{1\partial\phi}{D\partial x}\right)\right\}} \text{ Divergence}$$

$$\text{Coupling } \boxed{+\frac{\Delta\rho}{\rho o}g\left\{\frac{\partial}{\partial x}\left(\frac{h_2\partial\eta}{D\partial y}\right)-\frac{\partial}{\partial y}\left(\frac{h_2\partial\eta}{D\partial x}\right)\right\}} + \boxed{A_h\nabla^2 Z} \text{ Friction} \qquad (1)$$

Table 1. Parameters and model conditions for the experiments.

Runs	In- and outflow transport (Sv)	Bottom topographic parameter: α in (2)	Coefficient of horizontal eddy viscosity (A_h: cm^2sec^{-1})
B30T	30	1.0	10^7
B55T	55	1.0	10^7
B80T	80	1.0	10^7
B30T05	30	0.5	10^7
B55T05	55	0.5	10^7
B80T05	80	0.5	10^7
B30T01	30	0.1	10^7
B55T01	55	0.1	10^7
B80T01	80	0.1	10^7
B30T01E	30	0.1	5×10^6
B55T01E	55	0.1	5×10^6
B80T01E	80	0.1	5×10^6

m and actual depth D (in meter) for each run are given as

$$D=3800+\alpha(Dr-3800) \qquad (2)$$

where, Dr is the total depth of the realistic bottom topography shown in Fig. 1. In the first phase, the realistic bottom topography ($\alpha=1.0$) is given and three cases with different in- and outflow volume transport of 30, 55 and 80 Sv ($10^{12}cm^3sec^{-1}$) are performed (Table 1). These runs are referred to as B30T, B55T and B80T. In the second phase, because effect of the bottom topography has a tendency to be enhanced in a two layer model, six runs with small bottom slope ($\alpha=0.5$ and $\alpha=0.1$) are performed. Here, three different in- and outflow volume transport similar to the first phase are imposed and they are referred to as B30T05, B55T05 and B80T05 for runs with $\alpha=0.5$, and B30T01, B55T01 and B80T01 for runs with $\alpha=0.1$. In the third phase, although relatively large coefficient of horizontal eddy viscosity (A_h) of $10^7cm^2sec^{-1}$ are assumed for all the above runs, relatively small eddy viscosity with $A_h=5\times10^6cm^2sec^{-1}$ is given for this case. α is fixed to be 0.1 and three different in- and outflow similar to the previous cases are performed. So these runs are referred to as B30T01E, B55T01E and B80T01E.

3. Results

The results of B30T, B55T and B80T are shown Fig. 2. Main current path commonly flows along the northern boundary and large meander path is not formed. Three runs have similar velocity patterns and it is shown from the velocity fields of B80T (Fig. 3a) that the main current in the upper layer flows along the northern boundary and goes over the Izu Ridge. It is detected from the spacial distribution of the term balance in the vorticity equation (1) of B80T (Fig. 4) that main vorticity balance is made by divergence term and coupling term. This balance indicates the barotropic (divergence) and baroclinic (coupling) adjustment of the flow over the bottom slope. The upper layer mean flow over the continental slope is almost stable (e.g., SEKINE, 1992) and formation of large meander path is suppressed.

The results of B30T05, B55T05 and B80T05 are shown in Fig. 5. All the current paths flow along the northern boundary and large meander path is not formed. Almost similar results are obtained for B30T01, B55T01 and B80T01 shown in Fig. 6. It is shown from the vorticity balance of these models (not shown) that although the advection term is enlarged in comparison with the cases of $\alpha=1$, it is still smaller than the two bottom topographic terms and the vorticity balance is almost similar to that shown in Fig. 4. However, a different process is detected in early stage of B80T01 (Fig. 6c): the cyclonic circulation south of Shikoku is formed

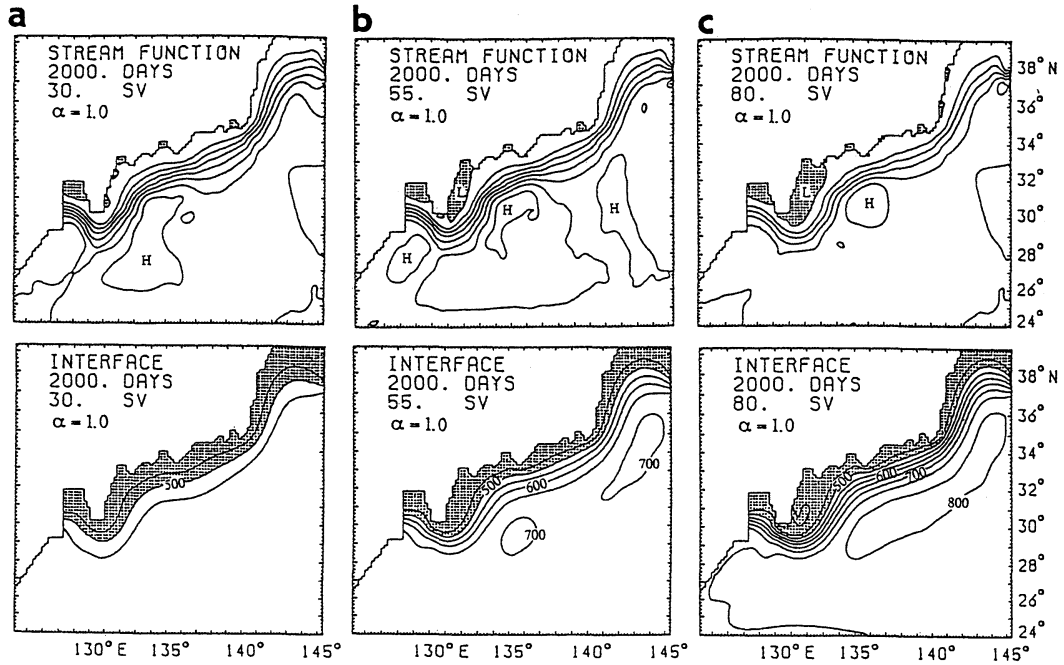

Fig. 2. Results of the cases with $\alpha = 1$ and $A_h = 10^7 cm^2 sec^{-1}$ shown by the isopleth of volume transport function (stream function) and upper layer thickness (interface). (a) B30T, (b) B55T and (c) B80T. The contour interval of the volume transport function is 5 Sv in (a), 10 Sv in (b) and 20 Sv in (c). Contour interval of the upper layer thickness is 50 m. Regions with negative volume transport function and those with the upper layer thickness thinner than 500 m are stippled.

by 100 days but decays in a short time. Furthermore, the anti-cyclonic circulation off Shikoku is advected eastward and a relatively large anti-cyclonic circulation is formed over the Izu ridge. During the advection of the anti-cyclonic circulation, the upper layer thickness does not correspond to the change in the volume transport function (Fig. 6d), which indicates that this processes is a barotropic phenomenon. It is suggested that the anti-cyclonic circulation off Shikoku is advected by the larger eastward mean flow and blocked by bottom topography of the Izu Ridge. It is also suggested that because the main flow runs rather northward in the eastern side of the Izu Ridge, the eastward advection of the anti-cyclonic circulation is suppressed by the weakened eastward flow.

Results of B30T01E, B55T01E and B80T01E with relatively small coefficient of horizontal eddy viscosity are shown in Fig. 7. Current paths of B30T01E and B55T01E (Fig. 7a,b) flow along the northern boundary and the straight path is formed. Eastward advection of the anti-cyclonic circulation off Shikoku, which is similar to B80T01 (Fig. 6c), occurs in B55T01E in periods of 300 ~ 550 days. In B80T01E (Fig. 7c), a cyclonic eddy east of Shikoku is formed and a stable large meander path is formed after about 250 days. The cyclonic eddy accompanied by the large meander path develops slightly upto about 1000 days. The velocity fields (Fig. 3d) show a different flow pattern from those of the above models: the main upper layer flow shows the separation in south of Kii Peninsula and significant cyclonic eddies and anti-cyclonic eddies are formed in the lower layer.

The time change kinetic energy in the lower layer is shown in Fig. 8. The kinetic energy of B80T, B80T05 and B80T01 attains stationary value in relatively early stage by about 300 days, however, that of B80T01E increases upto about 1000 days. Because the large meander

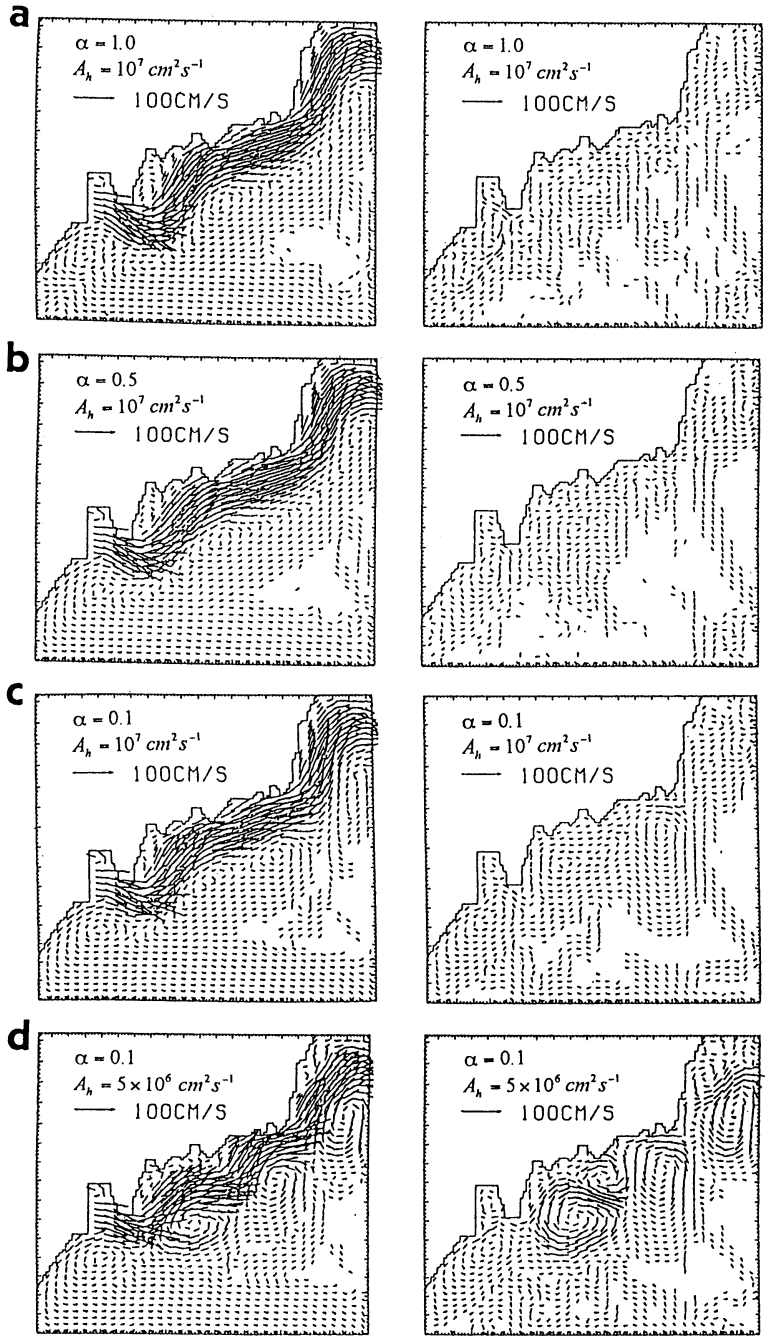

Fig. 3. Velocity fields in the upper (left) and lower (right) layer for the runs: (a) B80T, (b) B80T05, (c) B80T01 and (d) B80T01E. No velocity vectors less than 5 cm sec^{-1} are plotted.

path is formed before 1000 days, the large kinetic energy in the lower layer of B80T01E indicates the occurrence of baroclinic instability. The increase in the kinetic energy in the lower layer is also detected in B80T01, of which periods coincides with the development of the anti-

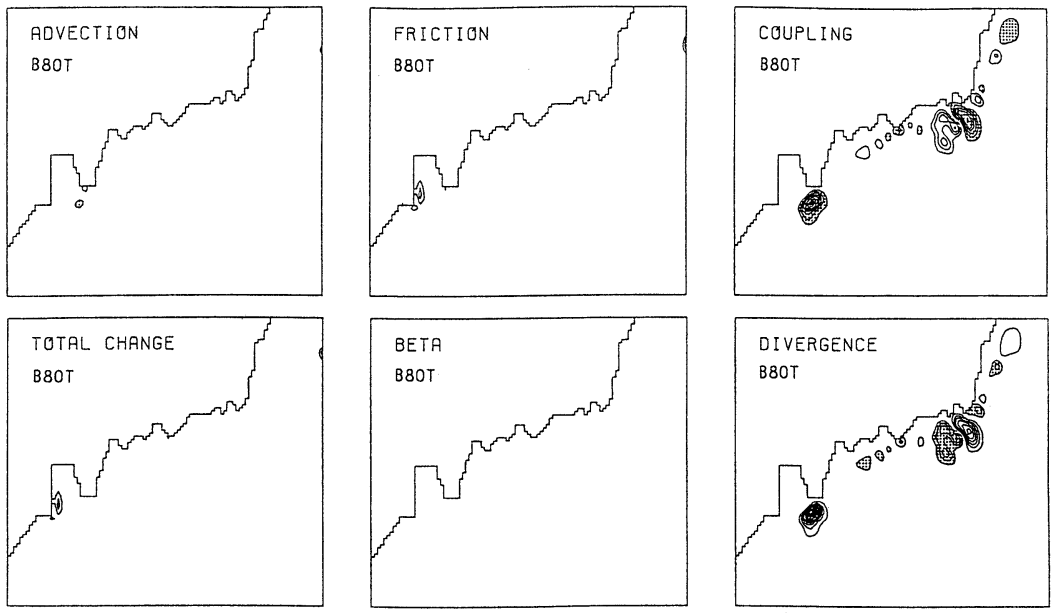

Fig. 4. Mean spatial balance of vorticity change estimated in the vorticity equation (1) for the case of B80T. Averaged values over 1500–2000 days are plotted. The contour interval is $7\times10^{11}\mathrm{sec}^{-2}$ and regions with negative vorticity change less than $-7\times10^{11}\mathrm{sec}^{-2}$ are stippled.

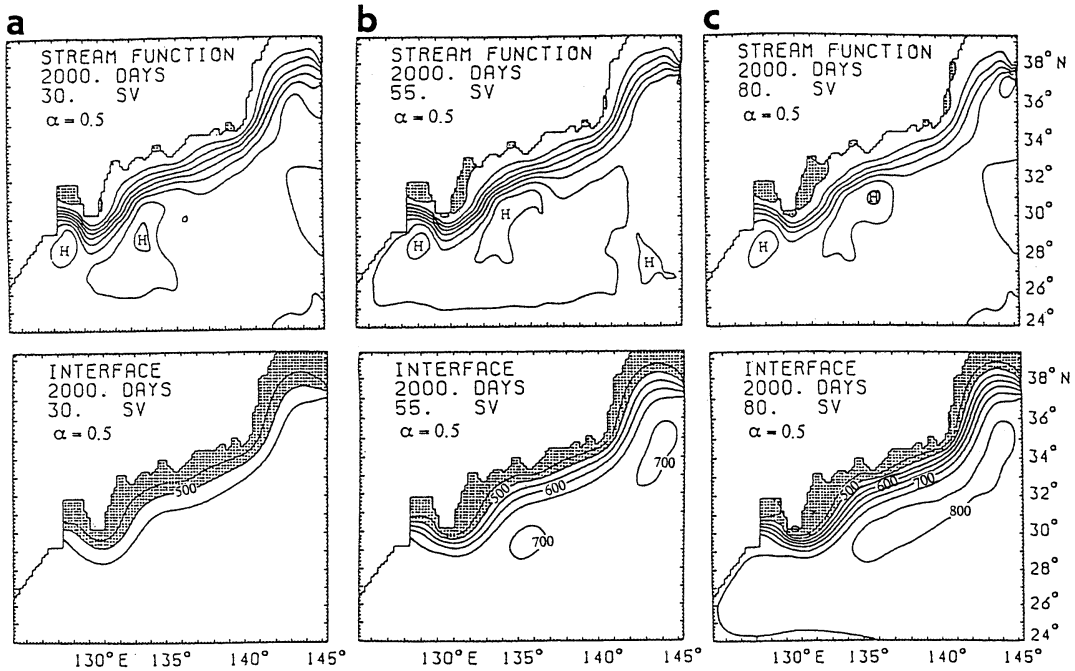

Fig. 5. Same as in Fig. 2 but for the runs with $\alpha=0.5$. (a) B30T05, (b) B55T05 and (c) B80T05.

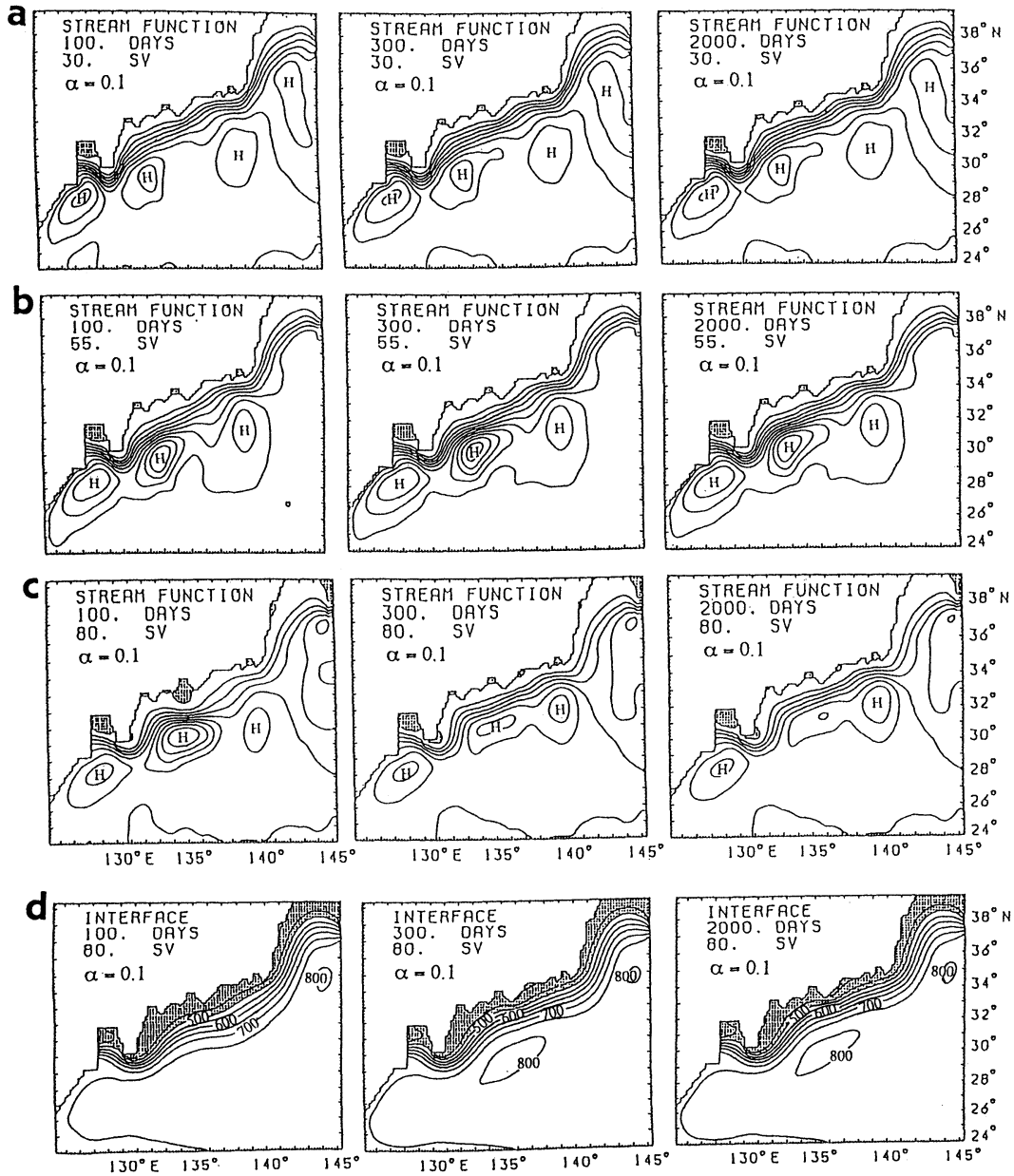

Fig. 6. Same as in Fig. 2 but for the runs with $\alpha = 0.1$. (a) B30T01, (b) B55T01 and (c) B80T01 and (d) the upper layer thickness of B80T01.

cyclonic eddy off Shikoku shown in Fig. 6c. However, the increase of the kinetic energy is ceased after 50 days, which indicates the finish of the occurrence of baroclinic instability. It is inferred that the ending of the baroclinic instability causes no occurrence of the large meander path in B80T01. It is shown from the velocity fields of B80T01E (Fig. 3d) that the cyclonic eddy south of Kii Peninsula is prominent in the lower layer, which agrees with the observational evidence (ISHII *et al.*, 1983; SEKINE *et al.*, 1985) that the cyclonic eddy accompanied

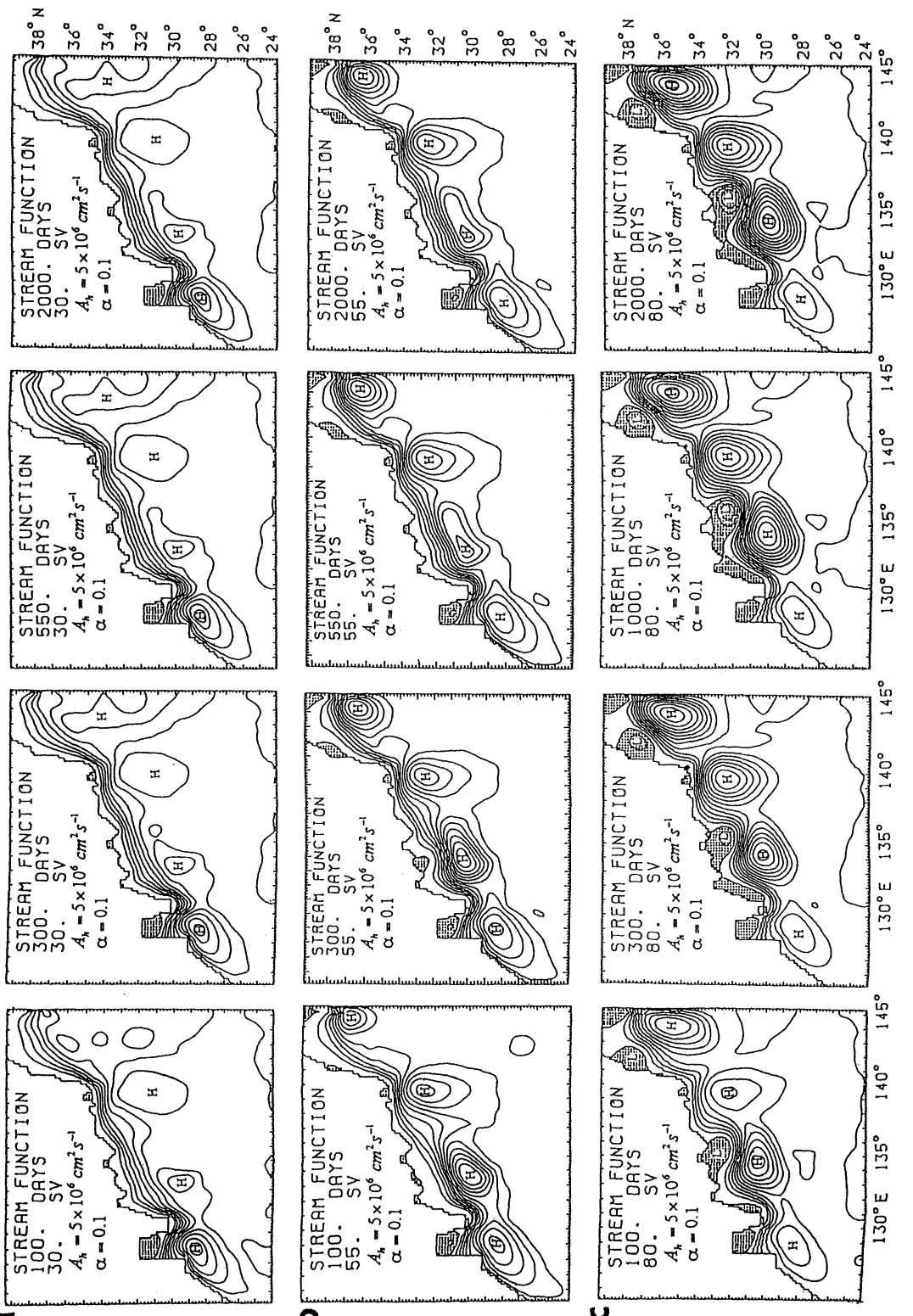

Fig. 7. Results of the runs with $\alpha = 0.1$ and $A_h = 5\times10^6 cm^2 sec^{-1}$. (a) B30T01E, (b) B55T01E and (c) B80T01E. The contour interval of the volume transport function is the same as Fig. 2.

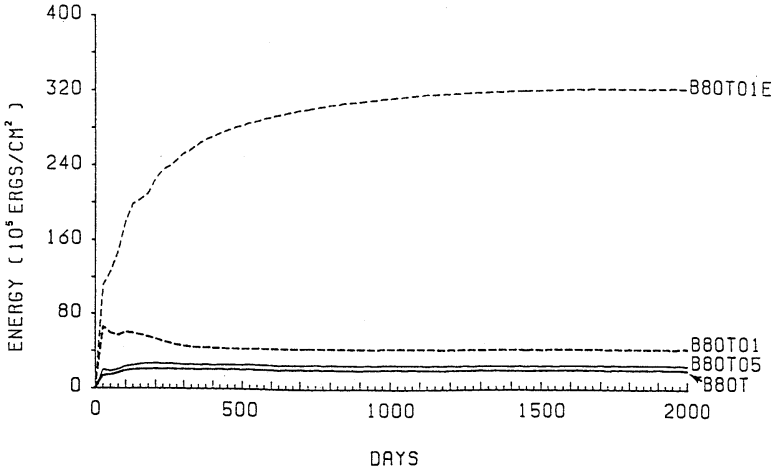

Fig. 8. Time change in mean kinetic energy in the lower layer defined by $\iint h_2(u_2^2+v_2^2)\,dxdy/\iint dxdy$, where the integration is carried out all over the model domain.

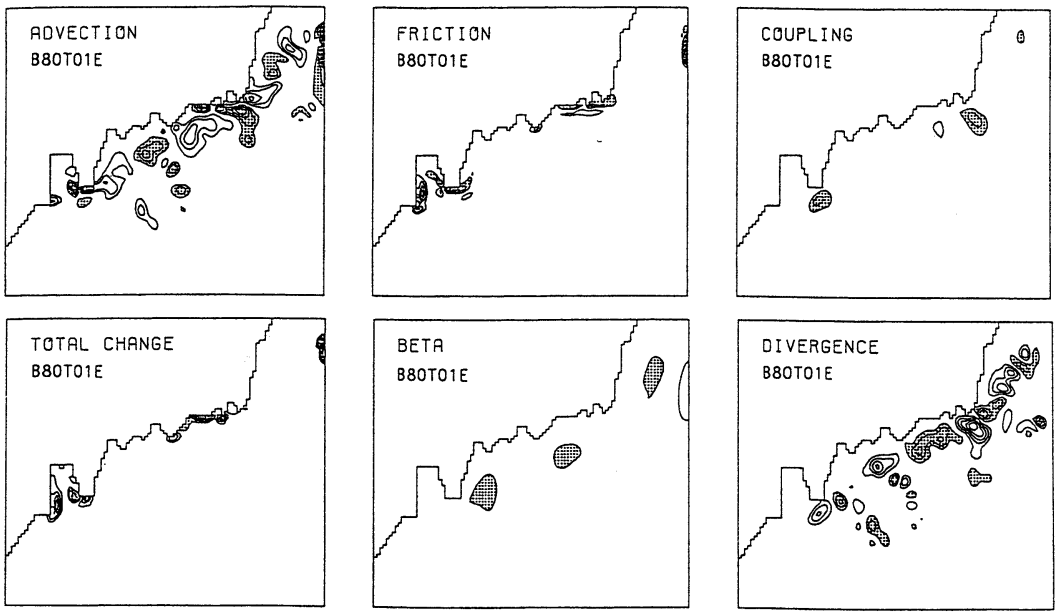

Fig. 9. Same as in Fig. 4 but for the case of B80T01E. Contour interval is $5\times10^{12}\text{sec}^{-2}$ and the region with less than $-5\times10^{12}\text{sec}^{-2}$ are stippled.

by the large meander path of the Kuroshio has a deep structure and it is not confined to the upper layer. It is suggested that the observed cyclonic flow structure in the deep layer is associated with the baroclinic instability of the mean flow.

The spatial distribution of the vorticity change in Eq. (1) of B80T01E is shown in Fig. 9. It should be noted that the dominant balance between divergence term and coupling term shown in Fig. 4 is weakened and the main balance is made among the advection, coupling and divergence term. It is resulted that large advective effect is further necessary for the formation of the large meander path.

4. Summary and discussion

As a succeeding study of Part 1 (ZHANG and

SEKINE, 1995), we have examined the bottom and coastal topographic effects on the path dynamics of the Kuroshio by use of a two-layer numerical model. The main results of the present study are summarized as follows:

(1) A straight path is formed in case with the realistic bottom topography ($\alpha=1$) and relatively large eddy viscosity ($A_h=10^7 cm^2 sec^{-1}$). It is shown from the vorticity balance that divergence term and coupling term are balanced, main flow in the upper layer over the continental slope is stabilized by the topographic effect of the bottom slope and the formation of large meander path is suppressed.

(2) A straight path is also formed in the cases with decreased bottom slope ($\alpha=0.5$ and 0.1) and relatively large eddy viscosity. In the run of B80T01, anti-cyclonic circulation off Shikoku is advected eastward and a relatively large anti-cyclonic circulation is formed over the Izu Ridge. This is due to the advection by large eastward mean flow and blocking by bottom topography of the Izu Ridge.

(3) A stable large meander path is formed in the case (B80T01E) of small eddy viscosity ($A_h=5\times10^6 cm^2 sec^{-1}$), small bottom slope of $\alpha=0.1$ and large in- and outflow volume transport (80 Sv). Large kinetic energy in the lower layer is generated in thes case, which indicates the occurrence of baroclinic instability. The main vorticity balance is made among divergence, coupling and advection terms. It is suggested that the baroclinic instability with strong inertial effect is necessary for the generation of large meander path under the stabilized effect of continental slope.

On the whole, the current path is stable and formation of large meander path is suppressed in comparison with the results of Part I. It is suggested by SEKINE (1992) that a flow over the continental slope south of Japan is almost stable by use of a simplified model proposed by IKEDA (1983). For the generation of a large meander path, a flow must go across isopleths of depth of the continental slope and large inertial effect is necessary. This causes the difference between the results of the present study and those of Part I. However, it is shown from this study that the topographic effect is weakened if the coefficient of horizontal eddy viscosity is decreased. Because observed flow character viewed from satellite imagery is generally perturbed more significantly than the flow pattern of B80T01E, it is indicated that more turbulent flow should be modeled in numerical experiment. To examine this point, a model with higer spatial resolution is necessary.

It was shown by Part I that a small meander southeast of Kyushu is stable and enhanced cyclonic eddy is formed on its coastal side. This result is not consistent with the observational evidence that almost of small meander off Kyushu decays in a several months (SEKINE and TOBA, 1981). However, because a few of the small meanders off Kyushu shifts eastward and develops into large meander path (e.g., SHOJI, 1972; KAWABE, 1980; SEKINE, 1992), time evolution of the small meander is very important for the path dynamics of the Kuroshio. In the present study, clear small meander with a cyclonic eddy off Kyushu is not simulated for all the cases. It is shown by SEKINE and TOBA (1981) that the formation of the small meander off Kyushu is carried out in periods of the increase in the Kuroshio velocity at the Tokara Strait. Although the time change in the volume transport is not considered in the present study, the time change in the volume transport (current velocity) is necessary for the simulation of dynamics of the Kuroshio south of Japan.

Acknowledgment

The authors would like to thank anonymous reviewer for his valuable comment. The numerical calculations were carried out on a VP-2600 in the Computer Center of Nagoya University and on a FACOM M-760 of Mie University Information Process Center. This study was supported by a Grant in Aid for Scientific Research Fund from Ministry of Education, Science and Culture of Japan (05640475).

References

AKITOMO, K., T. AWAJI and N. IMASATO (1991): Kuroshio path variation south of Japan. 1 Barotropic inflow-outflow model. J. Geophys. Res., **96**, 2549–2560.

CHAO, S-Y. and J. P. MCCREARY (1982): A numerical

study of the Kuroshio south of Japan. J. Phys. Oceanogr., **12**, 680–693.

CHAO, S-Y. (1984): Bimodality of the Kuroshio. J. Phys. Oceanogr., **14**, 92–103.

IKEDA, M. (1983): Linear instability of a current flowing along a bottom slope using a three layer model. J. Phys. Oceanogr., **13**, 208–223.

ISHII, H., Y. SEKINE and Y. TOBA (1983): Hydrostatic structure of the Kuroshio large meander-cold water mass region down to the deeper layers of the ocean. Journal of Oceanographical Society of Japan, **39**, 240–250.

KAWABE, M. (1980): Sea level variations around the Nansei Islands and the large meander path of the Kuroshio south of central Japan. J. Oceanogr. Soc. Japan, **36**, 227–235.

PEDLOSKY, J. (1979): "Geophysical fluid dynamics". Springer Verlag, New York, 624 pp.

SEKINE, Y. and Y. TOBA (1981): Velocity variation of the Kuroshio during formation of the small meander south of Kyushu. J. Oceanogr. Soc. Japan, **37**, 87–93.

SEKINE, Y., H. ISHII and Y. TOBA (1985): Spin-up and spin-down processes of the large cold water mass of the Kuroshio south of Japan. J. Oceanogr. Soc. Japan, **41**, 207–212.

SEKINE, Y. (1988): Coastal and bottom topographic effects on the Path dynamics of the western boundary current with special reference to the Kuroshio south of Japan. La mer, **26**, 99–114.

SEKINE, Y. (1990): A numerical experiment on the path dynamics of the Kuroshio with reference to the formation of the large meander path south of Japan. Deep-Sea Res., **37**, 359–380.

SEKINE, Y. (1992): On the signs of formation of the Kuroshio large meander south of Japan. Bull. Japan. Soc. Fish. Oceanogr., **56**, 13–22 (in Japanese with English abstract).

SHOJI, D. (1972): Time variation of the Kuroshio south of Japan. *In*: Kuroshio - Its physical aspects, H. Stommel and K. Yoshida, editors, Univ. Tokyo Press, pp. 165–214.

WHITE, W. B. and J. P. MCCREARY (1976): The Kuroshio meander and its relationship to the large scale ocean circulation. Deep-Sea Res., **23**, 33–47.

YAMAGATA, T. and S. UMATANI (1989): Geometry-forced coherent structure as a model of the Kuroshio large meander. J. Phys. Oceanogr., **19**, 234–242.

YOON, J. H. and I. YASUDA (1987): Dynamics of the Kuroshio large meander. Two-layer model. J. Phys. Oceanogr., **17**, 66–81.

ZHANG, M. and Y. SEKINE (1995): A numerical experiment on the path dynamics of the Kuroshio south of Japan. Part I Coastal topographic effect. La mer, **33**, 63–75.

日本南岸の黒潮流路の力学に関する数値実験

第2部　海底地形効果

張　銘秋・関根義彦

要旨：第1部の結果を基礎に，二層数値モデルを用いて日本南岸の黒潮流路の力学に関する陸岸及び海底地形効果を調べた．現実に近い日本南岸の陸岸・海底地形をモデル化し，海底地形の傾斜や流入出流量および水平渦粘性係数が異なる12のモデルを調べた．現実に近い海底地形と相対的に大きい渦粘性（$A_h=10^7 cm^2 sec^{-1}$）を与えたモデルでは岸に沿う流れが生じ，大蛇行流路は生じない．このモデルの渦度バランスでは発散項とカップリング項がバランスしており，陸棚斜面上の流路はほぼ安定であることが示された．同様な結果は海底地形傾斜を現実の半分または1/10にしたモデルでも得られた．しかし，渦粘性係数を小さくし（$A_h=5\times10^6 cm^2 sec^{-1}$）さらに海底地形傾斜を1/10，流入出流量が80 Svにしたモデルでは大蛇行の形成がみられた．このモデルでは傾圧不安定の発生で下層に大きな運動エネルギーが生じ，発散項とカップリング項と移流項がバランスしている．大蛇行流路は強い非線形（慣性）状態下の傾圧不安定で生じる可能性が示された．